







Rate-Splitting Assisted Cell-Free Symbiotic Radio: Channel Estimation and Transmission Scheme

Feiyang Li , Qiang Sun , *Member, IEEE*, Xiaomin Chen , *Member, IEEE*, Shuping Dang , *Senior Member, IEEE*, Jiayi Zhang , *Senior Member, IEEE*, and Kai-Kit Wong , *Fellow, IEEE*

Abstract—Cell-free symbiotic radio (CF-SR) is a promising technology to meet the demands of good quality-of-service and spectrum-efficient communications. However, the introduction of SR brings additional interference terms, which can seriously degrade the performance of the CF-SR systems. To suppress the interference, we adopt a rate-splitting (RS) transmission scheme to CF-SR. In this paper, we derive downlink spectral efficiency (SE) expressions of the CF-SR system with RS. Furthermore, in a conventional two-phase (TP) channel estimation scheme, the direct link causes heavy interference to the backscatter link, consequently diminishing the accuracy of the backscatter-link channel estimation. To this end, we propose a collaborative cancellation (CC) channel estimation scheme, which can eliminate the interference from the direct link and thus improve the accuracy of the backscatter-link channel estimation. Moreover, we derive the novel closed-form SE expressions under the CC channel estimation scheme using maximum ratio (MR) precoding. Simulation results show that the normalized mean square error (NMSE) of the CC channel estimation is consistently better than the one of the TP channel estimation, both on the direct and backscatter links. Furthermore, the advantages of the CC channel estimation scheme on the backscatter link can be further amplified in scenarios with a sufficient number of pilots. In addition, simulation results demonstrate that both the CC channel estimation scheme and the RS transmission scheme can provide significant improvements.

Index Terms—Cell-free massive MIMO, symbiotic radio, rate splitting, channel estimation, spectral efficiency.

I. INTRODUCTION

Cell-free massive multiple-input multiple-output (CF-mMIMO) is suggested as a prospective technology for beyond fifth-generation (B5G) and future wireless networks [1] [2]. In CF-mMIMO networks, a large number of access points (APs) are geographically distributed across the coverage area,

This work was supported in part by National Natural Science Foundation of China under Grant 62371262, 62401297 and 62341131, in part by the Key Research and Development Program of Nantong under Grant GZ2024002, in part by the Qinlan Project of Jiangsu Province, in part by the Scientific Research Program of Nantong under Grant JC22022026, and in part by the Postgraduate Research & Practice Innovation Program of Jiangsu Province under KYCX23_3399. (*Corresponding authors: Qiang Sun.*)

F. Li, Q. Sun, and X. Chen are with the School of Information Science and Technology, Nantong University, Nantong 226019, China. (e-mail: lfy@stmail.ntu.edu.cn; sunqiang@ntu.edu.cn; chenxm@ntu.edu.cn).

Shuping Dang is with School of Electrical, Electronic and Mechanical Engineering, University of Bristol, Bristol BS8 1UB, U.K. (e-mail: shuping.dang@bristol.ac.uk).

J. Zhang is with the School of Electronic and Information Engineering and the Frontiers Science Center for Smart High-speed Railway System, Beijing Jiaotong University, Beijing 100044, China. (e-mail: jiayizhang@bjtu.edu.cn).

K.-K. Wong is with the Department of Electronic and Electrical Engineering, University College London, London WC1E 6BT, U.K. (email: kitwong@ieee.org)

connecting to a central processing unit (CPU) via fronthaul links, and collectively provide coherent service to multiple user equipments (UEs) [3]. Similar to cellular massive MIMO, CF-mMIMO employs the favorable propagation and channel hardening properties when the number of APs is large to multiplex many UEs sharing the same time-frequency resource [4] [5]. Therefore, it can provide high spectral efficiency (SE) with simple signal processing [6] [7]. Nowadays, several works on CF-mMIMO focus on the maximum ratio (MR) processing [8] [9], while the work reported in [10] found that the higher SEs can be obtained when the minimum mean-square error (MMSE) processing is applied. In particular, by the CF-mMIMO configuration, the APs are placed close to the UEs, which yields a high macro-diversity and low path-loss fading [11]. As a result, numerous UEs can be served simultaneously with uniformly good quality-of-service [12]. However, the scarcity of radio spectrum resources remains a critical issue for CF-mMIMO [13]. In [14], the authors analyzed the user-driven minimum spectrum requirements based on challenging use cases developed from “day in the life” scenarios. The results show that even when considering only three key use cases, viz. healthcare, utilities, and motorway scenarios, approximately 76 GHz of spectrum resources may be needed if 0% spectrum sharing is implemented. Therefore, it is urgent to explore a spectral-efficient technology for the future CF-mMIMO.

The authors in [15] first proposed the symbiotic radio (SR) to address the challenge of scarce radio spectrum resources. The SR comprises a transmitter, a receiver, and a backscatter device (BD). The BD modulates information onto continuous wave signals generated by dedicated carrier emitters [16]. Moreover, the BD shares the same radio spectrum with the transmitter, and thus no dedicated spectrum is required [17] [18]. Therefore, SR can offer significant improvements in spectrum utilization for CF-mMIMO. Based on the above advantages, the integration of CF-mMIMO and SR has been studied in some works. Cell-free symbiotic radio (CF-SR) systems were first proposed in [19], in which a special case of a single UE under perfect channel state information (CSI) is considered. Furthermore, [20] and [21] investigated the CF-SR with multiple UEs under imperfect CSI. However, the multi-user interference remains a pressing issue for the CF-SR. The introduction of SR brings additional interference terms to CF-SR systems, which can seriously degrade the performance of CF-SR. Thus, it is crucial to develop a novel technique for effectively suppressing these interference.

Recently, rate-splitting (RS) has emerged as an effective solution for mitigating multi-user interference, particularly

in scenarios with imperfect CSI [22] [23]. This approach shows significant potential in counteracting the adverse effects associated with the introduction of SR in CF-mMIMO systems. Furthermore, RS can also relax the CSI quality requirements and expand the achievable rate region [24]. More specifically, a super common message is used to combine all these common streams. Then these message streams are transmitted simultaneously through the superposition coding. For the UE, the common message is decoded first, treating all private messages as noise. Following this, the desired private message can be decoded by removing the common message through successive interference cancellation (SIC) [25]. The appeal of RS lies in its ability to generalize two extreme existing approaches, i.e., treating interference as noise and utilizing interference for decoding, making it an attractive strategy for practical implementation [26]. For example, [27] introduced the concept of 1-layer RS strategy for downlink communications. The authors in [28] showed that rate-splitting multiple access (RSMA) can provide a smooth transition between space-division multiple access (SDMA) and non-orthogonal multiple access (NOMA) and outperforms them both in a wide range of network loads and user deployments. The benefits of transmitting multiple common streams were assessed for RSMA scheme in downlink multi-user systems [29]. The RS-aided beamforming scheme consistently outperforms NOMA in both partially and fully loaded systems [30]. Furthermore, in contrast to conventional linear precoding methods, non-orthogonal unicast and multicast transmission techniques supported by RS exhibit higher SE over a wide range of user deployment and network load scenarios [31] [32]. Besides the system-performance improvements, RS can offer additional benefits, e.g., relaxed CSI accuracy requirements and enhanced achievable rate regions [33] [39]. The application of RS in CF-mMIMO has been widely adopted to mitigate multi-user interference [35]–[37]. Despite these efforts, the current understanding of RS in mitigating multi-user interference in CF-SR systems remains incomplete and requires further investigation. It is important to note that, compared to traditional CF-mMIMO architectures, CF-SR introduces a substantial number of BDs for signal transmission. This could significantly increase multi-user interference and severely degrade SE.

Motivated by the above observations, we first analyze the downlink SE of CF-SR systems with pilot contamination. Then, to alleviate the multi-user interference in CF-SR systems, we implement RS based on the transmission of common and private messages. In addition, we propose a novel collaborative cancellation (CC) channel estimation scheme to improve the accuracy of the backscatter-link channel estimation. Finally, we propose a binary search method to find the appropriate power allocation (PA) factor for maximizing the sum SE of RS-assisted CF-SR systems. The major contributions of this paper are listed as follows:

- 1) We propose an RS-assisted CF-SR system model, where the channel from the UE and BD operates over Rician fading and the other channels operate over Rayleigh fading. The RS transmission scheme is employed to

mitigate the multi-user interference for enhancing the downlink SE. Moreover, a bisection search is utilized to determine the appropriate PA factor for maximizing the downlink sum SE.

- 2) Taking into account the interference on the backscatter link caused by the direct link, we propose a CC channel estimation scheme to improve the accuracy of the backscatter-link channel estimation. The simulation results demonstrate that the CC channel estimation scheme consistently outperforms the conventional two-phase (TP) channel estimation scheme in terms of the normalized mean square error (NMSE) for both direct and backscatter links. Furthermore, the advantages of the CC channel estimation scheme on the backscatter link can be further amplified in scenarios with a sufficient number of pilots.
- 3) By using the use-and-then-forget (UatF) bound, we derive achievable SE expressions for two transmission schemes, i.e., classical data transmission scheme and RS assisted CF-SR scheme, on both the direct and backscatter links. Note that our derived expressions hold for arbitrary precoding and channel estimation schemes. In addition, novel closed-form SE expressions with MR precoding schemes are calculated under the CC channel estimation scheme. The simulation results show that both the proposed CC channel estimation scheme and RS transmission scheme can provide significant improvements.

The rest of this paper is organized as follows. In Section II, we propose and describe the system model of CF-SR. Next, two channel estimation schemes are detailed in Section III. Then, two downlink data transmission schemes are proposed in Section IV. In Section V, simulation results are presented to compare the performance between the RS transmission scheme and the classical transmission scheme. Finally, Section VI concludes this paper.

Notation: Bold lowercase letters represent column vectors, while bold uppercase letters signify matrices. Superscripts $(\cdot)^*$, $(\cdot)^T$, and $(\cdot)^H$ indicate conjugate, transpose, and conjugate transpose, respectively. Symbol \triangleq is employed for definitions, and the identity matrix of size $N \times N$ is expressed as \mathbf{I}_N . The expected value of random variable \mathbf{g} is represented as $\mathbb{E}\{\mathbf{g}\}$.

II. SYSTEM MODEL

The proposed CF-SR system is illustrated in Fig. 1, in which a multitude of BDs are placed to assist in the wireless data transmission between the UEs and the APs. Here, K UEs, J BDs, and M APs are considered in the CF-SR system. All APs and UEs are equipped with a single antenna. It is assumed that the number of BDs is much larger than the number of UEs, and thus each UE can be paired with a different nearby BD, and the unselected BDs are not activated. More specifically, each activated BD is associated with one nearby UE to support the direct-link communications between the AP and UE. In addition, these BDs can also be used as extra APs, employing backscatter modulation to send their information to the UEs.

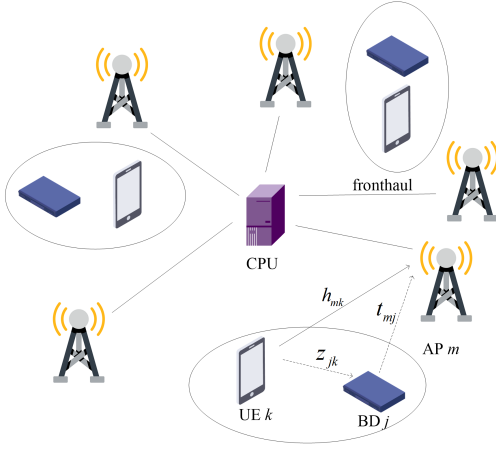


Fig. 1: CF-SR system model.

For simplicity, the selected BD near UE k is denoted as BD j .

All the APs are linked to a CPU via error-free fronthaul links and serve all UEs using the same time-frequency resource operating through the time-division duplex (TDD) protocol. The standard block fading model is applied in time-frequency blocks of τ_c channel uses. The direct-link channel with channel coefficient h_{mk} between UE k and AP m can be expressed as

$$h_{mk} = \beta_{mk}^{1/2} f_{mk}, \quad (1)$$

where $\beta_{mk} = \mathbb{E} \left\{ |h_{mk}|^2 \right\}$ characterizes the large-scale fading effects related to geometric path loss and shadowing, and $f_{mk} \sim \mathcal{CN}(0, 1)$ characterizes the small-scale fading effects; $t_{mj} \sim \mathcal{CN}(0, \beta_{mj})$ is utilized to signify the channel between AP m and BD j ; z_{jk} is used to denote the channel coefficient between UE k and BD j . Note that since UE k and BD j are relatively close to each other, the channel typically consists of a semideterministic line-of-sight (LoS) path and several reflection and scattering paths, which can thus be modelled as a Rician fading channel. Specifically, the channel coefficient between UE k and BD j is modelled as $z_{jk} \sim \mathcal{CN}(\Theta_{jk} \bar{z}_{jk}, \beta_{jk})$, where \bar{z}_{jk} represents the deterministic LoS component; $\Theta_{jk} \sim \mathcal{U}[-\pi, \pi]$ is the phase shift; β_{jk} models the large-scale fading effects on the non-LoS (NLoS) components. Thus, the total backscatter channel between AP m and UE k via BD j can be modeled as $g_{mk} = \alpha_j t_{mj} z_{jk}$, where α_j is the power reflection coefficient of BD j . Furthermore, we have $g_{mk} \sim \mathcal{CN}(0, \gamma_{mk})$ and $\gamma_{mk} = \mathbb{E} \left\{ |g_{mk}|^2 \right\}$.

If the symbol rate of the backscatter-link signals sent by BDs is significantly lower than that of the direct-link signals transmitted by APs, it facilitates an augmented synergy between the direct link and the backscatter link [15], thereby contributing to enhanced overall system performance. Therefore, we assume that each time BD j transmits a backscatter-link symbol to UEs, and AP m concurrently transmits L direct-link symbols. T_{dl} and T_{bl} represent the symbol periods of the UE and BD, respectively, given $T_{bl} = LT_{dl}$.

Fig. 2 shows the channel estimation and data transmission frame, in which each coherence interval is divided into two phases: the channel estimation phase taking $2\tau_p$ channel uses

and the downlink data transmission phase taking $\tau_c - 2\tau_p$ channel uses. It is required that $2\tau_p < \tau_c$.

III. CHANNEL ESTIMATION SCHEME

In the section, we describe two channel estimation schemes, namely, TP channel estimation and CC channel estimation, as shown in Fig. 2. TP channel estimation can bring additional interference from the direct link to the backscatter link, thus reducing the accuracy of the backscatter-link channel estimation. In contrast, CC channel estimation is expected to eliminate these aforementioned interferences.

A. Two-phase Channel Estimation

First, we present the TP channel estimation scheme, which has been widely applied in early papers [19]–[21]. In this scheme, the channel estimation procedure is divided into two phases, viz., the direct-link channel estimation phase and the backscatter-link channel estimation phase.

Let $\sqrt{\tau_p} \varphi_k^H \in \mathbb{C}^{\tau_p \times 1}$, where $\|\varphi_k\|^2 = 1$, denote the pilot sequence used by UE k . The allocation of these pilots to the UEs is deterministic but arbitrary. During the direct-link channel estimation phase, all UEs send pilot sequences of samples with length τ_p to all APs without activating BDs. Received signal $\mathbf{y}_{dl,m} \in \mathbb{C}^{\tau_p \times 1}$ at AP m is given by

$$\mathbf{y}_{dl,m} = \sqrt{\tau_p} \sum_{i=1}^K \sqrt{p_i^{ce}} h_{mi} \varphi_i^T + \mathbf{w}_{dl,m}, \quad (2)$$

where p_i^{ce} is the transmit power of UE i ; $\mathbf{w}_{dl,m} \sim \mathcal{CN}(\mathbf{0}, \sigma^2 \mathbf{I}_{\tau_p})$ represents the noise received at AP m , and σ^2 is the noise power. To estimate direct-link channel coefficient h_{mk} , AP m can correlate the received signal $\mathbf{y}_{dl,m}$ with pilot φ_k^* to obtain

$$\hat{y}_{dl,mk} = \sqrt{\tau_p p_k^{ce}} h_{mk} + \sqrt{\tau_p} \sum_{i \neq k} \sqrt{p_i^{ce}} h_{mi} \varphi_i^T \varphi_k^* + \mathbf{w}_{dl,m} \varphi_k^*. \quad (3)$$

Then, the direct-link channel estimation can be computed by using the standard MMSE estimation as

$$\hat{h}_{mk} = \frac{\mathbb{E} \left\{ \hat{y}_{dl,mk}^* h_{mk} \right\}}{\mathbb{E} \left\{ |\hat{y}_{dl,mk}|^2 \right\}} \hat{y}_{dl,mk} = \Xi_{mk} \hat{y}_{dl,mk}, \quad (4)$$

where

$$\Xi_{mk} \triangleq \frac{\sqrt{\tau_p p_k^{ce}} \beta_{mk}}{\tau_p \sum_{i=1}^K p_i^{ce} \beta_{mi} |\varphi_i^T \varphi_k^*|^2 + \sigma^2}. \quad (5)$$

After the standard MMSE estimation, the channel estimation error of direct link is defined as $\tilde{h}_{mk} = h_{mk} - \hat{h}_{mk}$, and, therefore, the average power of the channel estimation is given by

$$\hat{\beta}_{mk} = \mathbb{E} \left\{ |\hat{h}_{mk}|^2 \right\} = \sqrt{p_k^{ce} \tau_p} \beta_{mk} \Xi_{mk}. \quad (6)$$

Thus, we have $\tilde{h}_{mk} \sim \mathcal{CN}(0, \tilde{\beta}_{mk})$ and $\tilde{\beta}_{mk} = \beta_{mk} - \hat{\beta}_{mk}$. After the direct-link channel estimation phase, the backscatter-link channel estimation phase is performed. To estimate the

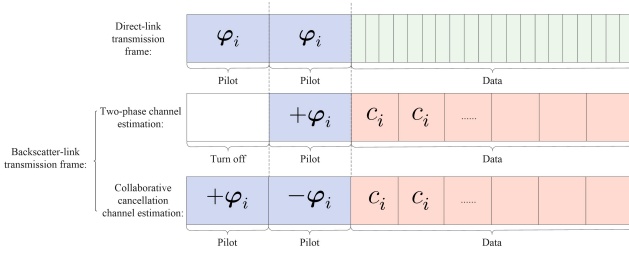


Fig. 2: Channel estimation and data transmission.

backscatter-link channel, all UEs are needed to retransmit the same pilot signals while the BDs are activated. Note that the pilot signals can be transmitted via both the direct-link and backscatter-link channels simultaneously. Pilot signals $\mathbf{y}'_{dl,m}$ received by AP m through the direct-link channel can thus be written as

$$\mathbf{y}'_{dl,m} = \sqrt{\tau_p} \sum_{i=1}^K \sqrt{p_i^{ce}} h_{mi} \varphi_i^T + \mathbf{w}_{bl,m}, \quad (7)$$

where $\mathbf{w}_{bl,m} \sim \mathcal{CN}(\mathbf{0}, \sigma^2 \mathbf{I}_{\tau_p})$ is the noise received at AP m in the backscatter-link channel estimation phase. Similarly, received pilot signals $\mathbf{y}_{BD,m}$ at AP m sent by the BD are given by

$$\mathbf{y}_{BD,m} = \sqrt{\tau_p} \sum_{i=1}^K \sqrt{p_i^{ce}} g_{mi} \varphi_i^T. \quad (8)$$

Finally, based on (7) and (8), total received signals $\mathbf{y}_{bl,m} \in \mathbb{C}^{\tau_p \times 1}$ at AP m can be determined as

$$\begin{aligned} \mathbf{y}_{bl,m} &= \mathbf{y}'_{dl,m} + \mathbf{y}_{BD,m} \\ &= \sqrt{\tau_p} \sum_{i=1}^K \sqrt{p_i^{ce}} h_{mi} \varphi_i^T + \sqrt{\tau_p} \sum_{i=1}^K \sqrt{p_i^{ce}} g_{mi} \varphi_i^T + \mathbf{w}_{bl,m}. \end{aligned} \quad (9)$$

Since estimated direct-link channel coefficients $\hat{\mathbf{h}}_{mk}$ have been calculated, the term related to $\hat{\mathbf{h}}_{mk}$ can be removed to improve the channel estimation accuracy. The signal after performing the removal, denoted as $\bar{\mathbf{y}}_{bl,m}$ can be written as

$$\begin{aligned} \bar{\mathbf{y}}_{bl,m} &= \mathbf{y}_{bl,m} - \sqrt{\tau_p} \sum_{i=1}^K \sqrt{p_i^{ce}} \hat{h}_{mi} \varphi_i^T \\ &= \sqrt{\tau_p} \sum_{i=1}^K \sqrt{p_i^{ce}} (\tilde{h}_{mi} + g_{mi}) \varphi_i^T + \mathbf{w}_{bl,m}. \end{aligned} \quad (10)$$

Improved signal $\bar{\mathbf{y}}_{bl,m}$ can be correlated with corresponding pilot signal φ_k^* to obtain

$$\begin{aligned} \hat{y}_{bl,mk} &= \bar{\mathbf{y}}_{bl,m} \varphi_k^* \\ &= \sqrt{\tau_p} \sum_{i=1}^K \sqrt{p_i^{ce}} (\tilde{h}_{mi} + g_{mi}) \varphi_i^T \varphi_k^* + \mathbf{w}_{bl,m} \varphi_k^*. \end{aligned} \quad (11)$$

Similar to the direct-link channel estimation phase, the MMSE estimation for backscatter-link channel coefficient g_{mk} can be

performed as

$$\hat{g}_{mk} = \frac{\mathbb{E} \left\{ \hat{y}_{bl,mk}^* g_{mk} \right\}}{\mathbb{E} \left\{ |\hat{y}_{bl,mk}|^2 \right\}} \hat{y}_{bl,mk} = \Psi_{mk} \hat{y}_{bl,mk}, \quad (12)$$

where

$$\Psi_{mk} \triangleq \frac{\sqrt{p_k^{ce}} \tau_p \gamma_{mk}}{\tau_p \sum_{i=1}^K p_i^{ce} (\tilde{\beta}_{mi} + \gamma_{mi}) |\varphi_i^T \varphi_k^*|^2 + \sigma^2}. \quad (13)$$

The average power of backscatter-link channel estimate \hat{g}_{mk} can be written as

$$\tilde{\gamma}_{mk} = \mathbb{E} \left\{ |\hat{g}_{mk}|^2 \right\} = \sqrt{p_k^{ce}} \tau_p \gamma_{mk} \Psi_{mk}. \quad (14)$$

In addition, we have $\tilde{g}_{mk} \sim \mathcal{CN}(0, \tilde{\gamma}_{mk})$ and $\tilde{\gamma}_{mk} = \gamma_{mk} - \hat{\gamma}_{mk}$.

Remark 1. As shown in (11), the received signal contains the residual signals from the direct link during the backscatter-link channel estimation phase. These residual signals are challenging to be completely removed but can be regarded as interference terms. Note that since the backscatter-link signal is significantly weaker than the direct-link signal, these interference terms could seriously degrade the accuracy of the backscatter-link channel estimation.

B. Collaborative Cancellation Channel Estimation

In this subsection, we propose a novel CC channel estimation, which can suppress the interference on the backscatter link caused by the direct link, and thus promote the accuracy of the backscatter-link channel estimation.

Similar to TP channel estimation, CC channel estimation is also divided into two phases. During the first phase, all UEs are required to transmit pilot signals with BDs activated. Despite being activated, BDs do not make any modulation in this phase. As a result, the received signal at AP m is analogous to (9) as

$$\mathbf{y}_{(1),m} = \sqrt{\tau_p} \sum_{i=1}^K \sqrt{p_i^{ce}} h_{mi} \varphi_i^T + \sqrt{\tau_p} \sum_{i=1}^K \sqrt{p_i^{ce}} g_{mi} \varphi_i^T + \mathbf{w}_{(1),m}, \quad (15)$$

where $\mathbf{w}_{(1),m} \sim \mathcal{CN}(\mathbf{0}, \sigma^2 \mathbf{I}_{\tau_p})$ denotes the received noise at AP m in the first channel estimation phase.

Then, we do not perform the channel estimation calculations but move to the second phase. During the second phase, all UEs retransmit the pilot signals while activating the BDs. Different from the first phase, the BDs need to modulate the amplitude of the received pilot signals, i.e., to assign “ $+\varphi$ ” to “ $-\varphi$ ”. Thus, the received signal at AP m is given by

$$\mathbf{y}_{(2),m} = \sqrt{\tau_p} \sum_{i=1}^K \sqrt{p_i^{ce}} h_{mi} \varphi_i^T - \sqrt{\tau_p} \sum_{i=1}^K \sqrt{p_i^{ce}} g_{mi} \varphi_i^T + \mathbf{w}_{(2),m}, \quad (16)$$

where $\mathbf{w}_{(2),m} \sim \mathcal{CN}(\mathbf{0}, \sigma^2 \mathbf{I}_{\tau_p})$ denotes the received noise at AP m in the second channel estimation phase.

After incorporating the received signals given in (15) and (16) into corresponding pilot signals φ_k^* , we have the equation

set as follows:

$$\begin{cases} y_{(1),m} = \sqrt{\tau_p} \sum_{i=1}^K \sqrt{p_i^{\text{ce}}} h_{mi} \varphi_i^T \varphi_k^* + \sqrt{\tau_p} \sum_{i=1}^K \sqrt{p_i^{\text{ce}}} g_{mi} \varphi_i^T \varphi_k^* + \mathbf{w}_{(1),m} \varphi_k^* \\ y_{(2),m} = \sqrt{\tau_p} \sum_{i=1}^K \sqrt{p_i^{\text{ce}}} h_{mi} \varphi_i^T \varphi_k^* - \sqrt{\tau_p} \sum_{i=1}^K \sqrt{p_i^{\text{ce}}} g_{mi} \varphi_i^T \varphi_k^* + \mathbf{w}_{(2),m} \varphi_k^* \end{cases} \quad (17)$$

With a series of simple addition and subtraction transformations, (17) can be simplified to

$$\begin{cases} \hat{y}_{(1),m} = \sqrt{\tau_p} \sum_{i=1}^K \sqrt{p_i^{\text{ce}}} h_{mi} \varphi_i^T \varphi_k^* + \frac{\mathbf{w}_{(1),m} \varphi_k^* + \mathbf{w}_{(2),m} \varphi_k^*}{2} \\ \hat{y}_{(2),m} = \sqrt{\tau_p} \sum_{i=1}^K \sqrt{p_i^{\text{ce}}} g_{mi} \varphi_i^T \varphi_k^* + \frac{\mathbf{w}_{(1),m} \varphi_k^* - \mathbf{w}_{(2),m} \varphi_k^*}{2} \end{cases} \quad (18)$$

Finally, by utilizing the standard MMSE estimation, the channel estimation of the direct link and backscatter link are obtained as follows. The channel estimates of h_{mk} and g_{mk} can be obtained as

$$\hat{h}_{mk} = \frac{\mathbb{E} \left\{ \hat{y}_{(1),m}^* h_{mk} \right\}}{\mathbb{E} \left\{ |\hat{y}_{(1),m}|^2 \right\}} \hat{y}_{(1),m} = \Xi_{mk} \hat{y}_{(1),m}, \quad (19)$$

and

$$\hat{g}_{mk} = \frac{\mathbb{E} \left\{ \hat{y}_{(2),m}^* g_{mk} \right\}}{\mathbb{E} \left\{ |\hat{y}_{(2),m}|^2 \right\}} \hat{y}_{(2),m} = \Psi_{mk} \hat{y}_{(2),m}, \quad (20)$$

where

$$\Xi_{mk} \triangleq \frac{\sqrt{\tau_p p_k^{\text{ce}}} \beta_{mk}}{\tau_p \sum_{i=1}^K p_i^{\text{ce}} \beta_{mi} |\varphi_i^T \varphi_k^*|^2 + \sigma^2/2}, \quad (21)$$

and

$$\Psi_{mk} \triangleq \frac{\sqrt{p_k^{\text{ce}}} \tau_p \gamma_{mk}}{\tau_p \sum_{i=1}^K p_i^{\text{ce}} \gamma_{mi} |\varphi_i^T \varphi_k^*|^2 + \sigma^2/2}. \quad (22)$$

Furthermore, the average power of the direct-link channel estimation and the backscatter-link channel estimation can be determined from the above estimates as $\hat{\beta}_{mk} = \mathbb{E} \left\{ |\hat{h}_{mk}|^2 \right\} = \sqrt{p_k^{\text{ce}}} \tau_p \beta_{mk} \Xi_{mk}$, and $\hat{\gamma}_{mk} = \mathbb{E} \left\{ |\hat{g}_{mk}|^2 \right\} = \sqrt{p_k^{\text{ce}}} \tau_p \gamma_{mk} \Psi_{mk}$, and the channel estimation errors of direct link and backscatter link can be written as $\tilde{g}_{mk} \sim \mathcal{CN}(0, \tilde{\gamma}_{mk})$, and $\tilde{h}_{mk} \sim \mathcal{CN}(0, \tilde{\beta}_{mk})$, where $\tilde{\gamma}_{mk} = \gamma_{mk} - \hat{\gamma}_{mk}$ and $\tilde{\beta}_{mk} = \beta_{mk} - \hat{\beta}_{mk}$, respectively¹.

Remark 2. Note that when channel estimation is performed, the BD can transmit at the same symbol period rate as the UE, which is the so-called parasitic SR in [17]. However, during the downlink transmission phase, the BD adopts a significantly lower symbol rate than that of the AP, thereby transitioning the system into a commensal SR system.

¹While the CC scheme is available for most situations, it still has some prerequisites to apply, e.g., precise time synchronization. Note that CC estimation scheme requires accurately capturing signals from two consecutive time slots. Misalignment of these time slots could result in signal conflicts, making it impossible to eliminate interference. Moreover, although the cancellation scheme is simple, it needs to be completed by the AP within a short period of time. Considering that the computational power of the AP is lower than that of the CPU, errors in calculations may occur, leading to imperfect cancellation.

IV. DOWNLINK DATA TRANSMISSION AND SPECTRAL EFFICIENCY ANALYSIS

In this section, we investigate the classical data transmission scheme and the RS assisted CF-SR transmission scheme. The SE expressions for both the direct and backscatter links are derived for both data transmission schemes.

A. Classical Data Transmission Scheme

We first consider the classical data transmission scheme, which has been adopted in previous papers [19]–[21]. During the downlink data transmission, we suppose that the APs treat the channel estimates as the true channel coefficients, thus the l th transmitted signal from AP m is given by

$$x_m(l) = \sum_{i=1}^K \sqrt{p_m} v_{mi} s_i(l), \quad (23)$$

where p_m denotes the transmit power of AP m ; v_{mk} is the local precoding coefficient; $s_i(l)$ represents the l th symbol intended for the i th UE, which satisfies $\mathbb{E} \left\{ |s_i(l)|^2 \right\} = 1$. Then the transmitted signal is received at the BDs and UEs. After receiving the transmitted signal, BD j modulates its own information over the signal by intentionally varying its reflection coefficient. Let u_i be the symbol sent by BD j , we consider symbol u_i to be modulated by binary phase-shift keying (BPSK), e.g., $u_i \in \{1, -1\}$. The l th received signals at UE k can be written as

$$\begin{aligned} r_k(l) &= \sum_{i=1}^K \sum_{m=1}^M \sqrt{p_m} v_{mi} h_{mk} s_i(l) \\ &+ \sum_{i=1}^K \sum_{m=1}^M \sqrt{p_m} v_{mi} g_{mk} s_i(l) u_i + n_k, \end{aligned} \quad (24)$$

where $n_k \sim \mathcal{CN}(0, \sigma^2)$ is the additive noise at UE k .

Two precoding mechanisms are considered in this paper, i.e., MR and local-MMSE (L-MMSE) precodings. Note that we refer to L-MMSE to distinguish it from MMSE, since each AP only knows its locally estimated channel information $\{\hat{h}_{mk}, \hat{g}_{mk} : m = 1, 2, \dots, M, k = 1, 2, \dots, K\}$ for precoding design with lower computational complexity. Owing to the uplink-downlink duality, we employ average-normalized precoding, and conjugate precoding v_{mk}^* is given by $v_{mk}^* = w_{mk} / \sqrt{\mathbb{E} \left\{ \|w_{mk}\|^2 \right\}}$. The term w_{mk} can be written as

$$w_{mk} = \begin{cases} \hat{h}_{mk} + \hat{g}_{mk}, & \text{for MR precoding} \\ p_{mk} \left(\sum_{i=1}^K p_{mi} \omega_{mi} + \sigma^2 \right)^{-1} (\hat{h}_{mk} + \hat{g}_{mk}) & \text{for L-MMSE precoding.} \end{cases} \quad (25)$$

where $\omega_{mi} = \hat{h}_{mi}^2 + \hat{g}_{mi}^2 + \tilde{\gamma}_{mi} + \tilde{\beta}_{mi}$. Note that the L-MMSE is calculated by minimizing the MSE, and $\text{MSE}_{mk} = \mathbb{E} \left\{ |s_k - v_{mk} r_k|^2 \mid \hat{h}_{mi}, \hat{g}_{mi} \right\}$.

Since direct-link signal s_i is significantly stronger than backscatter-link signal u_i , it is often decoded first. It is imperative to recognize that the symbol period of the APs

$$\text{SINR}_k^{\text{dl}} = \frac{|S_1 + S_2|^2}{\mathbb{E}\{|R_1|^2\} + \mathbb{E}\{|R_2|^2\} + \sum_{i \neq k}^K \mathbb{E}\{|R_3|^2\} + \sum_{i \neq k}^K \mathbb{E}\{|R_4|^2\} + \mathbb{E}\{|n_k|^2\}}. \quad (28)$$

is substantially lower than that of the BDs. Consequently, the second term in (24) can be constructed as the outcome of direct signal s_k propagating through a gradually varying channel characterized by channel coefficient $v_{mk}g_{mk}u_k$ [17]. Simultaneously, the signals emanating from other BDs are regarded as interference, and the average power of which is $\mathbb{E}\{p_m|v_{mi}|^2|g_{mk}|^2|s_i(l)|^2|u_i|^2\} = p_m|v_{mi}g_{mk}|^2$. Note that the knowledge of the channel estimates is not available; instead, we apply the UatF bound to calculate the achievable SE. To obtain the achievable SE, we rewrite (24) as

$$\begin{aligned} r_k(l) = & \mathbb{E}\left\{\underbrace{\sum_{m=1}^M \sqrt{p_m}v_{mk}h_{mk}}_{S_1}\right\} s_k(l) + \mathbb{E}\left\{\underbrace{\sum_{m=1}^M \sqrt{p_m}v_{mk}g_{mk}}_{S_2}\right\} s_k(l)u_k \\ & + \underbrace{\left(\sum_{m=1}^M \sqrt{p_m}v_{mi}h_{mk} - \mathbb{E}\left\{\sum_{m=1}^M \sqrt{p_m}v_{mk}h_{mk}\right\}\right)}_{R_1} s_k(l) \\ & + \underbrace{\left(\sum_{m=1}^M \sqrt{p_m}v_{mi}g_{mk} - \mathbb{E}\left\{\sum_{m=1}^M \sqrt{p_m}v_{mk}g_{mk}\right\}\right)}_{R_2} s_k(l)u_k \\ & + \underbrace{\sum_{i \neq k}^K \sum_{m=1}^M \sqrt{p_m}v_{mi}h_{mk} s_i(l)}_{R_3} + \underbrace{\sum_{i \neq k}^K \sum_{m=1}^M \sqrt{p_m}v_{mi}g_{mk} s_i(l)u_i}_{R_4} \\ & + n_k. \end{aligned} \quad (26)$$

Consequently, the downlink SE can be obtained by the following proposition:

Proposition 1. *The achievable downlink SE on the direct link for UE k is*

$$\text{SE}_k^{\text{dl}} = \left(1 - \frac{2\tau_p}{\tau_c}\right) \log_2 \left(1 + \text{SINR}_k^{\text{dl}}\right), \quad (27)$$

where the effective SINR is given by (28) (see top of this page).

Next, the backscatter-link signals are aspired to be decoded. To suppress the interference from the direct link, SIC is applied [17]. More specifically, the decoded direct-link signal $\sum_{i=1}^K \sum_{m=1}^M \sqrt{p_m}v_{mi}h_{mk}s_i(l)$ is subtracted from (24), yielding the intermediate signal as

$$r_k'(l) = r_k(l) - \sum_{i=1}^K \sum_{m=1}^M \sqrt{p_m}v_{mi}h_{mk}s_i(l). \quad (29)$$

Assuming on the imperfect SIC, the received signal given in

(24) can be simplified to

$$\begin{aligned} r_k'(l) = & \sum_{m=1}^M \sqrt{p_m}v_{mk}g_{mk}s_k(l)u_k \\ & + \sum_{i \neq k}^K \sum_{m=1}^M \sqrt{p_m}v_{mi}g_{mk}s_i(l)u_i \\ & + \sum_{i=1}^K \sum_{m=1}^M (\sqrt{p_m}v_{mi}h_{mk} \\ & - \mathbb{E}\{\sqrt{p_m}v_{mi}h_{mk}\})s_i(l) + n_k. \end{aligned} \quad (30)$$

Similar to (26), to obtain the achievable rate, (30) can be rewritten as

$$\begin{aligned} r_k'(l) = & \mathbb{E}\left\{\underbrace{\sum_{m=1}^M \sqrt{p_m}v_{mk}g_{mk}}_{S_2}\right\} s_k(l)u_k \\ & + \underbrace{\left(\sum_{m=1}^M \sqrt{p_m}v_{mi}g_{mk} - \mathbb{E}\left\{\sum_{m=1}^M \sqrt{p_m}v_{mk}g_{mk}\right\}\right)}_{R_2} s_k(l)u_k \\ & + \underbrace{\sum_{i \neq k}^K \sum_{m=1}^M \sqrt{p_m}v_{mi}g_{mk} s_i(l)u_i}_{R_4} + n_k \\ & + \underbrace{\sum_{i=1}^K \sum_{m=1}^M (\sqrt{p_m}v_{mi}h_{mk} - \mathbb{E}\{\sqrt{p_m}v_{mi}h_{mk}\})s_i(l)}_{R_5}. \end{aligned} \quad (31)$$

Since only one symbol from the backscatter link is transmitted during L successive symbol periods of the direct link, direct-link signal $s_k(l)$ can be seen as a spread-spectrum code with a length of L for backscatter signal u_k [15]. Consequently, the signal-to-interference-and-noise ratio (SINR) for decoding the backscatter signal increases by a factor of L , while the achievable SE decreases by $1/L$. Therefore, the achievable SE of the backscatter link can be expressed in Proposition 2 as follows:

Proposition 2. *The achievable downlink SE on the backscatter link for UE k is given by*

$$\text{SE}_k^{\text{bl}} = \left(1 - \frac{2\tau_p}{L\tau_c}\right) \log_2 \left(1 + \text{SINR}_k^{\text{bl}}\right), \quad (32)$$

where

$$\text{SINR}_k^{\text{bl}} = \frac{L|S_2|^2}{\mathbb{E}\{|R_2|^2\} + \sum_{i \neq k}^K \mathbb{E}\{|R_4|^2\} + \sum_{i=1}^K \mathbb{E}\{|R_5|^2\} + \mathbb{E}\{|n_k|^2\}}. \quad (33)$$

Remark 3. We observe that L-MMSE precoding coefficient v_{mk} can be designed to maximize the SINR of the direct link. Therefore, it may not be the optimal precoding for maximizing the SINR of the backscatter link. Nevertheless, it has been demonstrated in [21] that the suboptimal L-MMSE precoding still offers improved performance compared to the simple MR precoding.

B. Rate-Splitting Assisted CF-SR Transmission Scheme

In this subsection, we focus on the SE of RS-assisted CF-SR transmission. By treating the private messages as noise, we first derive the achievable SE expressions for the common messages on both the direct and backscatter links. After decoding the common messages, the remaining private messages are decoded by following the same steps as in the classical data transmission scheme.

We define W_k as the message the AP intends to send to the UE k , which is divided into a common part $W_{c,k}$ and a private part $W_{p,k}$. The common parts of all UEs, denoted as $\{W_{c,1}, W_{c,2}, \dots, W_{c,K}\}$, are amalgamated to constitute W_c . Employing a common codebook, W_c can be encoded into a common stream s_c with $\mathbb{E}\{|s_c|^2\} = 1$. Note that the common stream is designed for decoding by all UEs, though it may not be specifically targeted at each of them. The private part $W_{p,k}$ is independently encoded into a private stream s_k with $\mathbb{E}\{|s_k|^2\} = 1$. This stream is intended for decoding exclusively by the corresponding UE. Moreover, we presume that common message u_c and private message u_k sent by the BD also follow the aforementioned encoding principles. The signals sent by AP m can be written as

$$x_m(l) = \sqrt{p_{m,c}}v_{mc}s_c + \sum_{i=1}^K \sqrt{p_{m,p}}v_{mi}s_i, \quad (34)$$

where v_{mc} characterizes the common precoding; $p_{m,c}$ and $p_{m,p}$ are the power allocated to the common and private messages of AP m , respectively. Letting ρ ($0 \leq \rho \leq 1$) be the power splitting factor to adjust the fraction of the power allocated to the transmission of the common messages at each AP, we have $p_{m,c} = \rho p_m$ and $p_{m,p} = (1 - \rho)p_m$. If power splitting factor $\rho = 0$, the RS strategy is reduced to the classical data transmission scheme. After receiving these messages, BD j modulates the messages as

$$x_j(l) = \sqrt{p_{m,c}}v_{mc}s_c u_c + \sum_{i=1}^K \sqrt{p_{m,p}}v_{mi}s_i u_j. \quad (35)$$

Therefore, the l th received signal at UE k is given by

$$\begin{aligned} r_{k,c}(l) = & \sum_{m=1}^M \sqrt{p_{m,c}}v_{mc}h_{mk}s_c(l) + \sum_{m=1}^M \sqrt{p_{m,c}}v_{mc}g_{mk}s_c(l)u_c \\ & + \sum_{i=1}^K \sum_{m=1}^M \sqrt{p_{m,p}}v_{mi}h_{mk}s_i(l) \\ & + \sum_{i=1}^K \sum_{m=1}^M \sqrt{p_{m,p}}v_{mi}g_{mk}s_i(l)u_i + n_k. \end{aligned} \quad (36)$$

Note that common precoding v_{mc} is set as a linear sum of the private precoding coefficients, i.e., $v_{mc} = \sum_{i=1}^K v_{mi}$, to satisfy the decoding requirements of all UEs.

Proof: See Appendix B. ■

To decode the common signal on the direct link, we follow the same method as given in (26) to rewrite (36) as

$$\begin{aligned} r_{k,c}(l) = & \underbrace{\mathbb{E}\left\{\sum_{m=1}^M \sqrt{p_{m,c}}v_{mc}h_{mk}\right\}}_{S_1} s_c(l) \\ & + \underbrace{\mathbb{E}\left\{\sum_{m=1}^M \sqrt{p_{m,c}}v_{mc}g_{mk}\right\}}_{S_2} s_c(l)u_c \\ & + \underbrace{\left(\sum_{m=1}^M \sqrt{p_{m,c}}v_{mc}h_{mk} - \mathbb{E}\left\{\sum_{m=1}^M \sqrt{p_{m,c}}v_{mc}h_{mk}\right\}\right)}_{R_1} s_c(l) \\ & + \underbrace{\left(\sum_{m=1}^M \sqrt{p_{m,c}}v_{mc}g_{mk} - \mathbb{E}\left\{\sum_{m=1}^M \sqrt{p_{m,c}}v_{mc}g_{mk}\right\}\right)}_{R_2} s_c(l)u_c \\ & + \underbrace{\sum_{i=1}^K \sum_{m=1}^M \sqrt{p_{m,p}}v_{mi}h_{mk}}_{R_3} s_i(l) \\ & + \underbrace{\sum_{i=1}^K \sum_{m=1}^M \sqrt{p_{m,p}}v_{mi}g_{mk}}_{R_4} s_i(l)u_i + n_k. \end{aligned} \quad (37)$$

Remark 4. Although the simple common decoder has advantage of the low complexity, it cannot maximize the minimum SINR. For more insights, we refer interesting the readers to [36], which proposed a heuristic common precoder design aimed at maximizing the minimum SINR.

Then, the achievable SE for UE k is derived as follows:

Proposition 3. The achievable downlink SE on the direct link for UE k can be written as

$$\text{SE}_k^{c,\text{dl}} = \left(1 - \frac{2\tau_p}{\tau_c}\right) \log_2 \left(1 + \text{SINR}_k^{c,\text{dl}}\right), \quad (38)$$

where the SINR for the direct link can be written as (39)

Due to the fact that the direct-link common messages have been decoded, SIC can be applied to remove the interference. Therefore, (37) reduces to

$$\begin{aligned} r_{k,c}'(l) = & \underbrace{\mathbb{E}\left\{\sum_{m=1}^M \sqrt{p_{m,c}}v_{mc}g_{mk}\right\}}_{S_2} s_c(l)u_c \\ & + \underbrace{\sum_{i=1}^K \left(\sum_{m=1}^M \sqrt{p_{m,p}}v_{mi}h_{mk} - \mathbb{E}\left\{\sum_{m=1}^M \sqrt{p_{m,p}}v_{mi}h_{mk}\right\}\right)}_{R_1} s_i(l) \end{aligned} \quad (40)$$

$$\text{SINR}_k^{c,\text{dl}} = \frac{|S_1 + S_2|^2}{\mathbb{E}\{|R_1|^2\} + \mathbb{E}\{|R_2|^2\} + \sum_{i=1}^K \mathbb{E}\{|R_3|^2\} + \sum_{i=1}^K \mathbb{E}\{|R_4|^2\} + \mathbb{E}\{|n_k|^2\}}. \quad (39)$$

$$\begin{aligned} & + \underbrace{\left(\sum_{m=1}^M \sqrt{p_{m,c}} v_{mc} g_{mk} - \mathbb{E} \left\{ \sum_{m=1}^M \sqrt{p_{m,c}} v_{mc} g_{mk} \right\} \right)}_{R_2} s_c(l) u_c \quad \text{below:} \\ & + \underbrace{\sum_{i=1}^K \sum_{m=1}^M \sqrt{p_{m,p}} v_{mi} h_{mk} s_i(l)}_{R_3} \\ & + \underbrace{\sum_{i=1}^K \sum_{m=1}^M \sqrt{p_{m,p}} v_{mi} g_{mk} s_i(l) u_i + n_k}_{R_4}. \end{aligned} \quad (41)$$

Based on (40), the achievable downlink SE is determined as follows:

Proposition 4. *The achievable SE of the backscatter link for UE k is*

$$\text{SE}_k^{c,\text{bl}} = \left(1 - \frac{2\tau_p}{L\tau_c} \right) \log_2 \left(1 + \text{SINR}_k^{c,\text{bl}} \right), \quad (42)$$

where

$$\text{SINR}_k^{c,\text{bl}} = \frac{L|S_2|^2}{\sum_{i=1}^K \mathbb{E}\{|R_1|^2\} + \mathbb{E}\{|R_2|^2\} + \sum_{i=1}^K \mathbb{E}\{|R_3|^2\} + \sum_{i=1}^K \mathbb{E}\{|R_4|^2\} + \mathbb{E}\{|n_k|^2\}}. \quad (43)$$

After decoding all the common messages, SIC can be applied to remove the common messages. The residual signal is given by

$$\begin{aligned} r_{k,p}(l) &= \sum_{i=1}^K \sum_{m=1}^M \sqrt{p_{m,p}} v_{mi} h_{mk} s_i(l) \\ &+ \sum_{i=1}^K \sum_{m=1}^M \sqrt{p_{m,p}} v_{mi} g_{mk} s_i(l) u_i + n_k. \end{aligned} \quad (44)$$

From the above derivations, it is clear that the form of residual signal (44) is similar to (24); thus we can adopt the same steps to decode the direct-link and backscatter-link signals. Following similar steps to the classical transmission scheme, the achievable SEs on both the direct and backscatter links are derived as follows.

Proposition 5. *The achievable SEs on the direct link and backscatter link for UE k can be written as*

$$\text{SE}_k^{p,\text{dl}} = \left(1 - \frac{2\tau_p}{\tau_c} \right) \log_2 \left(1 + \text{SINR}_k^{p,\text{dl}} \right), \quad (45)$$

and

$$\text{SE}_k^{p,\text{bl}} = \left(1 - \frac{2\tau_p}{L\tau_c} \right) \log_2 \left(1 + \text{SINR}_k^{p,\text{bl}} \right), \quad (46)$$

where the instantaneous SINR is given in (47) and (48) (see top of the next page).

The detailed expressions for the above terms are illustrated

$$S_1 = \mathbb{E} \left\{ \sum_{m=1}^M \sqrt{p_{m,p}} v_{mk} h_{mk} \right\}, \quad (49)$$

$$S_2 = \mathbb{E} \left\{ \sum_{m=1}^M \sqrt{p_{m,p}} v_{mk} g_{mk} \right\}, \quad (50)$$

$$R_1 = \sum_{m=1}^M \sqrt{p_{m,p}} v_{mk} h_{mk} - \mathbb{E} \left\{ \sum_{m=1}^M \sqrt{p_{m,p}} v_{mk} h_{mk} \right\}, \quad (51)$$

$$R_2 = \sum_{m=1}^M \sqrt{p_{m,p}} v_{mk} g_{mk} - \mathbb{E} \left\{ \sum_{m=1}^M \sqrt{p_{m,p}} v_{mk} g_{mk} \right\}, \quad (52)$$

$$R_3 = \sum_{m=1}^M \sqrt{p_{m,p}} v_{mi} h_{mk}, \quad (53)$$

$$R_4 = \sum_{m=1}^M \sqrt{p_{m,p}} v_{mi} g_{mk}, \quad (54)$$

$$R_5 = \sum_{m=1}^M \sqrt{p_{m,c}} v_{mc} h_{mk} - \mathbb{E} \left\{ \sum_{m=1}^M \sqrt{p_{m,c}} v_{mc} h_{mk} \right\}, \quad (55)$$

$$R_6 = \sum_{m=1}^M \sqrt{p_{m,c}} v_{mc} g_{mk} - \mathbb{E} \left\{ \sum_{m=1}^M \sqrt{p_{m,c}} v_{mc} g_{mk} \right\}, \quad (56)$$

and

$$R_7 = \sum_{m=1}^M \sqrt{p_{m,p}} v_{mi} h_{mk} - \mathbb{E} \left\{ \sum_{m=1}^M \sqrt{p_{m,p}} v_{mi} h_{mk} \right\} \quad (57)$$

In addition, the expectations of the SINR cannot be derived in closed-form when applying L-MMSE precoding, but can be calculated by using Monte Carlo sampling. Meanwhile, we can obtain the following closed-form expression when utilizing MR precoding and CC channel estimation:

Corollary 1. *If MR precoding $v_{mk} = \hat{h}_{mk} + \hat{g}_{mk} / \sqrt{\mathbb{E}\{\|\hat{h}_{mk} + \hat{g}_{mk}\|^2\}}$ and CC channel estimation are applied, the expectations of closed-form can be written as*

$$\mathbb{E}\{v_{mk} h_{mk}\} = \frac{\hat{\beta}_{mk}}{\sqrt{\hat{\beta}_{mk} + \hat{\gamma}_{mk}}} \beta_{mk}, \quad (58)$$

$$\mathbb{E}\{v_{mk} g_{mk}\} = \frac{\hat{\gamma}_{mk}}{\sqrt{\hat{\beta}_{mk} + \hat{\gamma}_{mk}}}, \quad (59)$$

$$\mathbb{E} \left\{ \left| \sum_{m=1}^M v_{mi} h_{mk} \right|^2 \right\} = \sum_{m=1}^M \frac{\hat{\beta}_{mi} \beta_{mk}}{\hat{\beta}_{mi} + \hat{\gamma}_{mi}} + \sum_{m=1}^M \frac{\hat{\gamma}_{mi} \beta_{mk}}{\hat{\beta}_{mi} + \hat{\gamma}_{mi}} \quad (60)$$

$$\text{SINR}_k^{p,\text{dl}} = \frac{|S_1 + S_2|^2}{\mathbb{E}\{|R_1|^2\} + \mathbb{E}\{|R_2|^2\} + \sum_{i \neq k}^K \mathbb{E}\{|R_3|^2\} + \sum_{i \neq k}^K \mathbb{E}\{|R_4|^2\} + \mathbb{E}\{|R_5|^2\} + \mathbb{E}\{|R_6|^2\} + \mathbb{E}\{|n_k|^2\}} \quad (47)$$

$$\text{SINR}_k^{p,\text{bl}} = \frac{L|S_2|^2}{\mathbb{E}\{|R_2|^2\} + \sum_{i \neq k}^K \mathbb{E}\{|R_4|^2\} + \mathbb{E}\{|R_5|^2\} + \mathbb{E}\{|R_6|^2\} + \sum_{i=1}^K \mathbb{E}\{|R_7|^2\} + \mathbb{E}\{|n_k|^2\}} \quad (48)$$

$$+ \left| \sum_{m=1}^M \frac{\hat{\beta}_{mi}\beta_{mk}}{\beta_{mi}\sqrt{\hat{\beta}_{mi} + \hat{\gamma}_{mi}}} \right|^2 |\varphi_i^T \varphi_k^*|^2, \quad (61)$$

and

$$\mathbb{E} \left\{ \left| \sum_{m=1}^M v_{mi} g_{mk} \right|^2 \right\} = \sum_{m=1}^M \frac{\hat{\gamma}_{mi}\gamma_{mk}}{\hat{\beta}_{mi} + \hat{\gamma}_{mi}} + \sum_{m=1}^M \frac{\hat{\beta}_{mi}\gamma_{mk}}{\hat{\beta}_{mi} + \hat{\gamma}_{mi}} \quad (62)$$

$$+ \left| \sum_{m=1}^M \frac{\hat{\gamma}_{mi}\gamma_{mk}}{\gamma_{mi}\sqrt{\hat{\beta}_{mi} + \hat{\gamma}_{mi}}} \right|^2 |\varphi_i^T \varphi_k^*|^2. \quad (63)$$

Proof: See Appendix A. ■

Remark 5. It can be seen that the closed-form expressions of SINR change with the channel estimation scheme. We also refer the readers to [21] for more insights into the closed-form expressions under TP channel estimation.

C. Power Allocation Factor to Maximize the Downlink Sum SE

After all the messages are decoded from the received signals given in (36), the downlink sum SE can be defined as

$$\text{SSE} = \min(\text{SE}_k^c) + \sum_{i=1}^K \text{SE}_i^p. \quad (64)$$

Note that we adopt the commensal SR approach for transmission, whereby the enhancement of backscatter-link signals also yields performance gains for the direct link. As a result, we can optimize the sum SE of the backscatter link while concurrently elevating the sum SE of the direct link. Therefore, the optimization problem can be formulated as

$$\max_{\{\rho\}} \text{SSE}^{\text{bl}} = \min(\text{SE}_k^{\text{c,bl}}) + \sum_{i=1}^K \text{SE}_i^{p,\text{bl}} \quad (65)$$

subject to $0 \leq \rho \leq 1$.

It is evident that as power allocation factor ρ increases, the SE of the common messages experiences an increase, while that of the private messages undergoes a decrease. Consequently, the downlink sum SE follows a monotonic trend, indicating the existence of an appropriate ρ that maximizes it. Thus, adjusting the power allocation factor is crucial for unleashing the full potential of RS technology. It is worth

Algorithm 1 Proposed Binary Search Algorithm for Solving (65)

Result: the power splitting factor ρ .

Input: SSE^{bl} , the tolerance ε , the minimum value ρ_{\min} , and the maximum value ρ_{\max} .

Initialization: Set the initial values $\rho_{\min} = 0$ and $\rho_{\max} = 1$;

Set the tolerance $\varepsilon > 0$ and an increase $0 < \Delta\rho \ll \varepsilon$;

$\text{SSE}_{\max}^{\text{bl}} = \text{SSE}^{\text{bl}}(\rho^*) =$

$\max\left\{\left[\text{SSE}^{\text{bl}}(\rho_{\min}), \text{SSE}^{\text{bl}}(\rho_{\max})\right]\right\}$ and $\rho = \rho^*$;

while $\rho_{\max} - \rho_{\min} > \varepsilon$ **do**

Set $\rho_{\text{next}} = (\rho_{\max} + \rho_{\min})/2$;

$\text{SSE}_{\text{next}}^{\text{bl}} = \text{SSE}^{\text{bl}}(\rho_{\text{next}})$ and $\text{SSE}_{\Delta}^{\text{bl}} =$

$\text{SSE}^{\text{bl}}(\rho_{\text{next}} + \Delta\rho)$;

If $\text{SSE}_{\Delta}^{\text{bl}} > \text{SSE}_{\text{next}}^{\text{bl}}$, then set $\rho_{\min} = \rho_{\text{next}}$, else set

$\rho_{\max} = \rho_{\text{next}}$;

If $\text{SSE}_{\text{next}}^{\text{bl}} > \text{SSE}_{\max}^{\text{bl}}$, then set $\text{SSE}_{\max}^{\text{bl}} = \text{SSE}_{\text{next}}^{\text{bl}}$ and

$\rho = \rho_{\text{next}}$;

end while

Output: ρ .

noting that (65) can be solved efficiently by a bisection search, in each step solving a sequence of convex feasibility problems.

Binary search is an algorithm used to locate the position of a target value within a sorted array. The algorithm compares the target value to the middle element of the array. If they are not equal, the half, in which the target value cannot be located, is eliminated. The search then continues on the remaining half, again comparing the target value to the middle element. This process is repeated until the target value is found. By consistently eliminating the half, in which the target value cannot lie, the algorithm efficiently narrows down the search area in each iteration [38]. The steps for solving (65) are summarized in Algorithm 1.

V. NUMERICAL RESULTS

A. Simulation Setup and Radio Propagation Model

In this section, we numerically evaluate the performance of the CF-SR system under different channel estimation and data transmission schemes. We consider that M APs and K UEs are uniformly distributed in a 1×1 km² area with a wrap-around method. From [15] and [20], we suppose each BD is located at the area of a circle centered at its associated device with a radius of d_{jk}^{max} .

TABLE I: Simulation Parameters

Parameter	Value
Communication bandwidth	20 MHz
AP antenna height	10 m
Noise power, σ^2	-94 dBm
Circling distance, d_{jk}^{\max}	0.5 m
Coherence time, τ_c	200 msec
Uplink training duration, τ_p	4 msec
Power reflection coefficient, α	1
Number of APs, M	100
Number of UEs, K	8
Number of BDs, J	8
Transmission period, L	20
Uplink transmit power per UE, p_k^{ce}	20 dBm
Downlink transmit power per AP, p_m	20 dBm

For large-scale fading, we apply the classical 3GPP Urban Microcell model [10], in which the large-scale fading factor is given by

$$\beta_{xy}[\text{dB}] = -30.5 - 36.7 \log_{10} \left(\frac{d_{xy}}{1 \text{ m}} \right) + Q_{xy}, \quad (66)$$

where d_{xy} denotes the 3D distance between AP x and UE/BD y , which accounts for the border wraparound and AP antenna mounted at a height of 10 m. Moreover, $Q_{xy} \sim \mathcal{CN}(0, 4^2)$ reflects the shadow fading, and the shadowing terms between AP l and different UEs are stipulated by

$$\mathbb{E} \{Q_{kl}Q_{ij}\} = \begin{cases} 4^2 2^{-\delta_{ki}/9} \text{ m}, & l = j \\ 0, & l \neq j \end{cases}, \quad (67)$$

where δ_{ki} is the distance between UE k and UE i . The second term in (67) characterizes the correlation of shadowing terms associated with two distinct APs. This correlation is negligible due to the simulation setup, where there is a minimum separation of at least 50 m between adjacent APs.

Furthermore, for the large-scale fading between the BDs and the APs, we instead utilize the propagation model applied in [20]:

$$\beta_{jk}[\text{dB}] = -26 - 20 \log_{10} \left(\frac{d_{jk}}{1 \text{ m}} \right), \quad (68)$$

where d_{jk} denotes the distance between BD j and UE k . From [39] and [40], large-scale coefficient of channel h_{jk} between BD j and UE k can be written as

$$\beta_{jk}^{\text{LoS}} = \frac{\kappa_{jk}}{\kappa_{jk} + 1} \beta_{jk}, \quad \beta_{jk}^{\text{NLoS}} = \frac{1}{\kappa_{jk} + 1} \beta_{jk}, \quad (69)$$

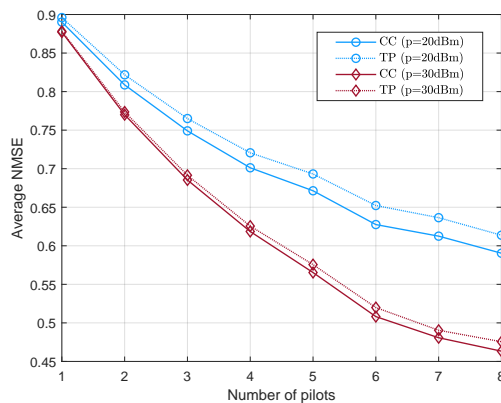
where $\kappa_{jk} = 10^{1.3 - 0.003d_{jk}}$ is the Rician κ -factor.

All simulation parameters are shown in Table I.

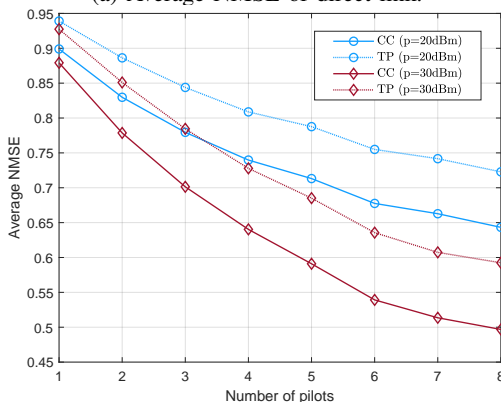
B. Normalized Mean Square Error of Channel Estimation

In this section, the NMSE is calculated to compare the accuracy of different channel estimation schemes, which is defined as

$$\text{NMSE}_{mk}^{\text{dl}} = \frac{\tilde{\beta}_{mk}}{\beta_{mk}} \quad \text{and} \quad \text{NMSE}_{mk}^{\text{bl}} = \frac{\tilde{\gamma}_{mk}}{\gamma_{mk}}, \quad (70)$$



(a) Average NMSE of direct link.



(b) Average NMSE of backscatter link.

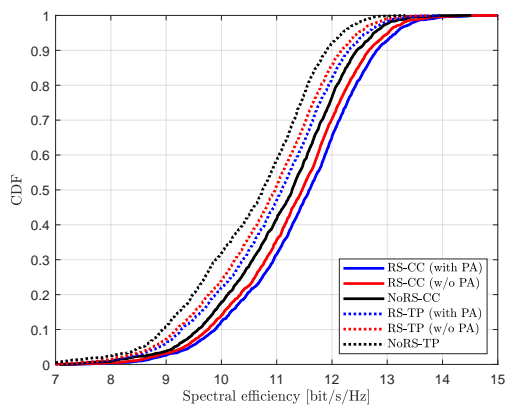
Fig. 3: Average NMSE with CC/TP channel estimation under different uplink training duration and downlink transmission power when $K = 8$.

for both direct and backscatter links. Note that the values of NMSE fall within the range of 0 to 1. A value of 0 indicates perfect estimation, while a value of 1 signifies extremely impaired estimation.

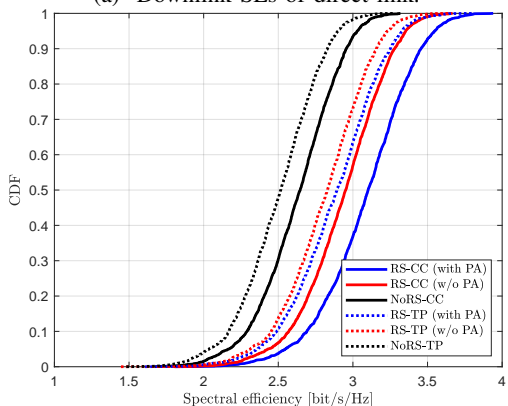
Fig. 3 compares the NMSE of TP and CC channel estimations with different uplink training duration and downlink transmission power. It is clear that the NMSE of CC channel estimation is consistently better than that of the TP channel estimation, both on the direct and backscatter links. We also find that the advantage of CC channel estimation on the backscatter link can be further amplified when the number of pilots is sufficient. In addition, the superiority of CC channel estimation on the direct link decreases when the downlink transmit power increases. This is due to the increase in the signal-to-noise ratio (SNR), and thus the effect of noise becomes negligible.

C. SE of Different Transmission Schemes

Fig. 4 shows the cumulative distribution function (CDF) of the downlink sum SE for the proposed system under CC/TP channel estimation with L-MMSE precoding. It is evident that RS yields about 10% improvements on both the direct and backscatter links, surpassing scenarios where RS is not employed. This is due to the fact that RS allows a portion of the total downlink power to be allocated to the common



(a) Downlink SEs of direct link.



(b) Downlink SEs of backscatter link.

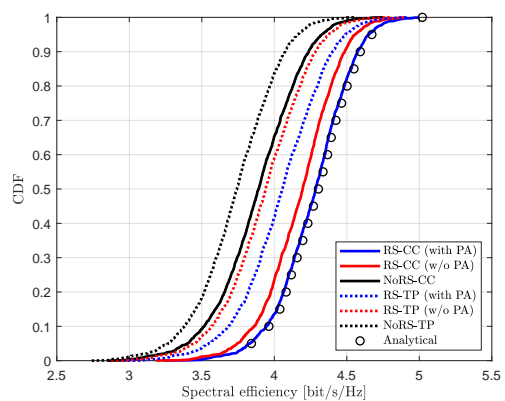
Fig. 4: Downlink SEs per UE with L-MMSE precoding when $M = 100$ and $K = 8$.

message, especially when imperfect CSI is taken into account. Consequently, this allocation empowers RS to manage interference more effectively on the UE side. Furthermore, it can be found that compared to the direct link, RS can bring larger performance gains to the backscatter link. This is because the backscatter link is more severely impacted by double-fading attenuation and imperfect SIC, resulting in weak interference suppression capabilities. In addition, the proposed CC channel estimation method can achieve about 8% gains on both direct and backscatter links.

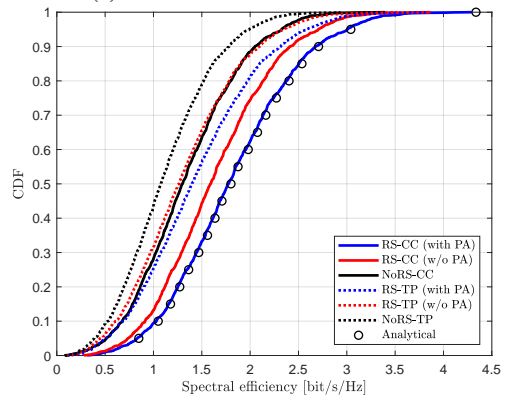
Fig. 5 examines the same setups but with MR precoding $v_{mk} = \hat{h}_{mk} + \hat{g}_{mk}$. Different from Fig. 4, all cases lose SEs due to poor precoding schemes. Since MR precoding cannot suppress residual interference due to imperfect SIC, there is around 40% performance loss on the backscatter link. However, the proposed RS method and CC channel estimation scheme can achieve larger SEs. Moreover, the gains of PA increase compared to Fig. 4, which verifies the effectiveness of PA in the absence of interference immunity. Besides, markers “o” generated by analytical results overlap with the curves generated by simulations, validating the accuracy of our derived closed-form SE expressions.

D. Effects of Uplink Training Duration

In CF-mMIMO systems, ensuring pilot sequence orthogonality can consume a significant portion of the coherence time,



(a) Downlink SEs of direct link.



(b) Downlink SEs of backscatter link.

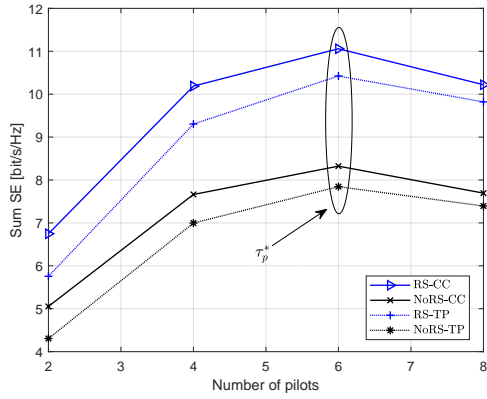
Fig. 5: Downlink SEs per UE with MR precoding when $M = 100$ and $K = 8$.

potentially impacting system performance. This challenge is exacerbated in CF-SR setups, where the employed channel estimation scheme necessitates twice the coherence time compared to CF-mMIMO systems. Therefore, it is essential to find optimal point τ_p^* when coherence time τ_c is not long enough.

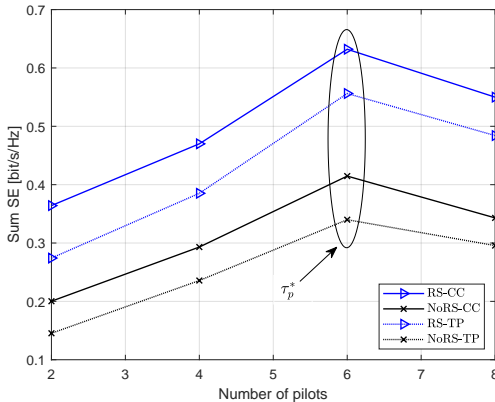
Fig. (6) depicts the average SE with L-MMSE precoding. The parameters are set as $M = 100$, $K = 20$, and $\tau_c = 50$ unit of time is required. In Fig. (6), we find that the performance of direct link relies more on the accuracy of channel estimation compared to backscatter link; hence the SE is rather low when the number of pilots is small. Furthermore, we observe that the SEs of direct and backscatter links reduce with the increase of τ_p after reaching the maximum SE value at τ_p^* . Besides, the CC channel estimation can consistently provide a higher average SE than the TP channel estimation, regardless of the number of pilots. These crucial insights also validate that augmenting training duration τ_p is not always beneficial; as such, an increase in the training duration may result in a deterioration of the data transmission duration.

E. Effects of Symbiotic Radio

Note that the SR can provide an additional link, which can be viewed as the output of the direct-link signal passing through a slowly varying channel. Nevertheless, it also brings additional interference terms to the system. Thus, it is necessary to compare the SE performance between the CF-SR network and the conventional CF network.



(a) Sum downlink SEs of direct link.



(b) Sum downlink SEs of backscatter link.

Fig. 6: Sum downlink SEs when $M = 100$, $K = 8$, and $\tau_c = 50$ unit of time is required.

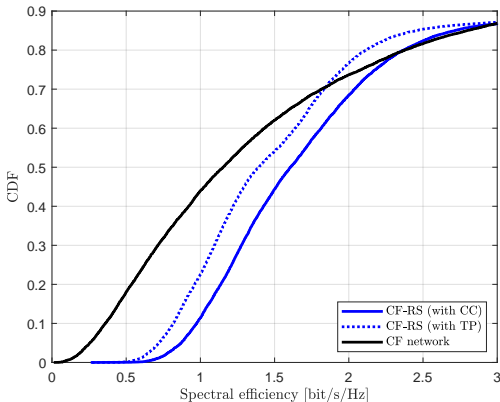


Fig. 7: Downlink SEs with L-MMSE precoding when $M = 100$ and $K = 8$.

Fig. 7 presents the CDF of the downlink SE for the proposed CF-SR and CF network without RS. Despite the additional interference, the CF-SR under TP channel estimation still yields about 0.5 bit/s/Hz improvements over 95% SE span. This improvement is further amplified when using CC channel estimation, as it enhances the accuracy of the channel estimation.

VI. CONCLUSION

In this paper, we conducted an investigation into the downlink performance of CF-SR with RS. We proposed a CC channel estimation method to improve the accuracy of the backscatter-link channel estimation. Furthermore, we derived novel closed-form SE expressions under the CC channel estimation scheme using the MR precoding. In addition, we also proposed a bisection search method to determine the optimal PA factor for maximizing the downlink sum SE. Through simulation results, we compared the performance of the two downlink transmission schemes and channel estimation schemes. Notably, the NMSE of CC channel estimation is consistently better than the TP channel estimation, both on the direct and backscatter links. Moreover, the advantages of the CC channel estimation scheme on the backscatter link can be further amplified in scenarios with a sufficient number of pilots. Numerical results presented in this paper showed that the proposed CC channel estimation scheme and RS transmission scheme can provide about 8% and 9% improvement, respectively. To summarize, our findings clearly demonstrate that both the RS transmission scheme and the CC channel estimation scheme can bring superior performance to CF-SR.

APPENDIX

A. Proof of Corollary 1

To derive the closed-form expression, we need to calculate $\mathbb{E}\{v_{mk}h_{mk}\}$, $\mathbb{E}\{v_{mk}g_{mk}\}$, $\mathbb{E}\left\{\left|\sum_{m=1}^M v_{mi}h_{mk}\right|^2\right\}$, and $\mathbb{E}\left\{\left|\sum_{m=1}^M v_{mi}g_{mk}\right|^2\right\}$ as follows:

$$\begin{aligned} & \mathbb{E}\{v_{mk}h_{mk}\} \\ &= \frac{1}{\sqrt{\hat{\beta}_{mk} + \hat{\gamma}_{mk}}} \mathbb{E}\left\{\sum_{m=1}^M \hat{h}_{mk}(\hat{h}_{mk} + \tilde{h}_{mk}) + \sum_{m=1}^M \hat{g}_{mk}(\hat{h}_{mk} + \tilde{h}_{mk})\right\} \\ &\stackrel{(a)}{=} \frac{1}{\sqrt{\hat{\beta}_{mk} + \hat{\gamma}_{mk}}} \mathbb{E}\left\{\sum_{m=1}^M \hat{h}_{mk}\hat{h}_{mk} + \sum_{m=1}^M \hat{g}_{mk}(\hat{h}_{mk} + \tilde{h}_{mk})\right\} \\ &\stackrel{(b)}{=} \sum_{m=1}^M \frac{\hat{\beta}_{mk}}{\sqrt{\hat{\beta}_{mk} + \hat{\gamma}_{mk}}}, \end{aligned} \tag{71}$$

where (a) and (b) hold because \tilde{h}_{mk} and \hat{g}_{mk} are independent of \hat{h}_{mk} and h_{mk} ;

$$\begin{aligned} & \mathbb{E}\left\{\left|\sum_{m=1}^M v_{mi}h_{mk}\right|^2\right\} \\ &= \mathbb{E}\left\{\left|\sum_{m=1}^M \frac{h_{mk}(\hat{h}_{mi} + \hat{g}_{mi})}{\sqrt{\hat{\beta}_{mi} + \hat{\gamma}_{mi}}}\right|^2\right\} \\ &\stackrel{(c)}{=} \mathbb{E}\left\{\left|\sum_{m=1}^M \frac{h_{mk}\hat{h}_{mi}}{\sqrt{\hat{\beta}_{mi} + \hat{\gamma}_{mi}}}\right|^2\right\} + \mathbb{E}\left\{\left|\sum_{m=1}^M \frac{h_{mk}\hat{g}_{mi}}{\sqrt{\hat{\beta}_{mi} + \hat{\gamma}_{mi}}}\right|^2\right\} \end{aligned}$$

$$= \mathbb{E} \left\{ \left| \sum_{m=1}^M \frac{h_{mk} \hat{h}_{mi}}{\sqrt{\hat{\beta}_{mi} + \tilde{\gamma}_{mi}}} \right|^2 \right\} + \sum_{m=1}^M \frac{\beta_{mk} \hat{\gamma}_{mi}}{\hat{\beta}_{mi} + \tilde{\gamma}_{mi}}, \quad (72)$$

where the cross term in (c) is small and can thus be omitted, and similar cases are treated in the same manner in the subsequent proofs;

$$\begin{aligned} & \mathbb{E} \left\{ \left| \sum_{m=1}^M h_{mk} \hat{h}_{mi} \right|^2 \right\} \\ &= \mathbb{E} \left\{ \left| \sqrt{\tau_p} \sum_{m=1}^M \sum_{k'=1}^K \sqrt{p_{k'}^{ce}} h_{mk} \Xi_{mi} h_{mk'} \varphi_{k'}^T \varphi_k^* \right|^2 \right\} \\ &+ \mathbb{E} \left\{ \left| \sum_{m=1}^M h_{mk} \Xi_{mi} \left(\frac{\mathbf{w}^{(1),m} \varphi_k^* + \mathbf{w}^{(2),m} \varphi_k^*}{2} \right) \right|^2 \right\} \\ &= \mathbb{E} \left\{ \left| \sqrt{\tau_p} \sum_{m=1}^M \sum_{k'=1}^K \sqrt{p_{k'}^{ce}} h_{mk} \Xi_{mi} h_{mk'} \varphi_{k'}^T \varphi_k^* \right|^2 \right\} \\ &+ \frac{\sigma^2}{2} \sum_{m=1}^M \beta_{mk} \Xi_{mi}^2, \end{aligned} \quad (73)$$

and

$$\mathbb{E} \left\{ \left| \sqrt{\tau_p} \sum_{m=1}^M \sum_{k'=1}^K \sqrt{p_{k'}^{ce}} h_{mk} \Xi_{mi} h_{mk'} \varphi_{k'}^T \varphi_k^* \right|^2 \right\} \quad (74)$$

$$= p_i^{ce} \tau_p |\varphi_i^T \varphi_k^*|^2 \mathbb{E} \left\{ \left| \sum_{m=1}^M h_{mk}^2 \Xi_{mi} \right|^2 \right\} \quad (75)$$

$$+ \tau_p \mathbb{E} \left\{ \left| \sum_{m=1}^M \sum_{k' \neq i}^K \sqrt{p_{k'}^{ce}} h_{mk} \Xi_{mi} h_{mk'} \varphi_{k'}^T \varphi_k^* \right|^2 \right\}, \quad (76)$$

where

$$\begin{aligned} & \mathbb{E} \left\{ \left| \sum_{m=1}^M h_{mk}^2 \Xi_{mi} \right|^2 \right\} \\ &= \mathbb{E} \left\{ \sum_{m=1}^M \sum_{n=1}^M h_{nk}^2 h_{mk}^2 \Xi_{ni} \Xi_{mi} \right\} \\ &= \mathbb{E} \left\{ \sum_{m=1}^M |h_{mk}^2 \Xi_{mi}|^2 \right\} + \mathbb{E} \left\{ \sum_{m=1}^M \sum_{n \neq m}^M h_{nk}^2 h_{mk}^2 \Xi_{ni} \Xi_{mi} \right\} \\ &= 2 \sum_{m=1}^M \beta_{mk}^2 \Xi_{mi}^2 + \sum_{m=1}^M \sum_{n \neq m}^M \beta_{mk}^2 \beta_{nk}^2 \Xi_{ni} \Xi_{mi}. \end{aligned} \quad (77)$$

Similarly, we have

$$\begin{aligned} & \mathbb{E} \left\{ \left| \sum_{m=1}^M \sum_{k' \neq i}^K \sqrt{p_{k'}^{ce}} h_{mk} \Xi_{mi} h_{mk'} \varphi_{k'}^T \varphi_k^* \right|^2 \right\} \\ &= \sum_{m=1}^M \sum_{k' \neq i}^K \sqrt{p_{k'}^{ce}} \beta_{mk} \beta_{mk'} \Xi_{mi}^2 |\varphi_{k'}^T \varphi_k^*|^2. \end{aligned} \quad (78)$$

Based on the (73), (74), (77), and (78), we have

$$\begin{aligned} \mathbb{E} \left\{ \left| \sum_{m=1}^M v_{mi} h_{mk} \right|^2 \right\} &= \sum_{m=1}^M \frac{\hat{\beta}_{mi} \beta_{mk}}{\hat{\beta}_{mi} + \tilde{\gamma}_{mi}} + \sum_{m=1}^M \frac{\beta_{mk} \hat{\gamma}_{mi}}{\hat{\beta}_{mi} + \tilde{\gamma}_{mi}} \\ &+ \left| \sum_{m=1}^M \frac{\hat{\beta}_{mi} \beta_{mk}}{\beta_{mi} \sqrt{\hat{\beta}_{mi} + \tilde{\gamma}_{mi}}} \right|^2 |\varphi_i^T \varphi_k^*|^2. \end{aligned} \quad (79)$$

Finally, follow the similar steps as above, the closed-form expressions of $\mathbb{E} \left\{ \left| \sum_{m=1}^M v_{mi} g_{mk} \right|^2 \right\}$ and $\mathbb{E} \{v_{mk} g_{mk}\}$ can be obtained.

B. Proof of Common Precoding

The total signals from AP m and the corresponding BD is given by

$$\begin{aligned} r_{mk} &= \sqrt{p_{m,c}} h_{mk} s_c + \sqrt{p_{m,c}} g_{mk} s_c u_c \\ &+ \sum_{i=1}^K \sqrt{p_{m,p}} h_{mk} s_i + \sum_{i=1}^K \sqrt{p_{m,p}} h_{mk} s_i u_i + n_k. \end{aligned} \quad (80)$$

Thus, MSE_{mk} is

$$\begin{aligned} \text{MSE}_{mk} &= \mathbb{E} \left\{ |s_c - v_{mk} r_{k,c}|^2 \mid \hat{h}_{mi}, \hat{g}_{mi} \right\} \\ &= p_{m,c} - 2p_{m,c} v_{mk} \hat{h}_{mk} - 2p_{m,c} v_{mk} \hat{g}_{mk} \\ &+ v_{mk}^* \left(\sum_{i=1}^K p_{m,p} (\hat{h}_{mi}^2 + \hat{g}_{mi}^2 + \tilde{\gamma}_{mi} + \tilde{\beta}_{mi}) + \sigma^2 \right) v_{mk}. \end{aligned} \quad (81)$$

By introducing notation $a_{mk} = p_{m,c} \hat{h}_{mk} + p_{m,c} \hat{g}_{mk}$ and $c_{mk} = \sum_{i=1}^K p_{m,p} (\hat{h}_{mi}^2 + \hat{g}_{mi}^2 + \tilde{\gamma}_{mi} + \tilde{\beta}_{mi}) + \sigma^2$, MSE_{mk} can be rewritten as

$$\begin{aligned} \text{MSE}_{mk} &= p_{m,c} - 2v_{mk} a_{mk} + v_{mk}^* c_{mk} v_{mk} \\ &= p_{m,c} - a_{mk}^* c_{mk}^{-1} a_{mk} \\ &+ (v_{mk} - c_{mk}^{-1} a_{mk})^* c_{mk} (v_{mk} - c_{mk}^{-1} a_{mk}). \end{aligned} \quad (82)$$

Note that MSE_{mk} is minimized with respect to v_{mk} when the last term is zero, which occurs when $v_{mk} = c_{mk}^{-1} a_{mk}$.

REFERENCES

- [1] X. Chen, D. W. K. Ng, W. Yu, E. G. Larsson, N. Al-Dhahir, and R. Schober, "Massive access for 5G and beyond," *IEEE J. Sel. Areas Commun.*, vol. 39, no. 3, pp. 615-637, Sep. 2021.
- [2] H. A. Ammar, R. Adve, S. Shahbazpanahi, G. Boudreau, and K. V. Srinivas, "User-centric cell-free massive MIMO networks: A survey of opportunities, challenges and solutions," *IEEE Commun. Surveys Tuts.*, vol. 24, no. 1, pp. 611-652, 1st Quart., 2022.
- [3] T. Zhao, X. Chen, Q. Sun, and J. Zhang, "Energy-efficient federated learning over cell-free IoT networks: Modeling and optimization," *IEEE Internet Things J.*, vol. 10, no. 19, pp. 17436-17449, Oct. 2023.
- [4] J. Zhang, J. Zhang, E. Björnson, and B. Ai, "Local partial zero-forcing combining for cell-free massive MIMO systems," *IEEE Trans. Commun.*, vol. 69, no. 12, pp. 8459-8473, Dec. 2021.
- [5] Z. Wang, J. Zhang, B. Ai, C. Yuen, and M. Debbah, "Uplink performance of cell-free massive MIMO with multi-antenna users over jointly correlated Rayleigh fading channels," *IEEE Trans. Wireless Commun.*, vol. 21, no. 9, pp. 7391-7406, Sep. 2022.

- [6] J. Zhang *et al.*, "Prospective multiple antenna technologies for beyond 5G," *IEEE J. Sel. Areas Commun.*, vol. 38, no. 8, pp. 1637-1660, Aug. 2020.
- [7] J. Zhang, J. Zhang, D. W. K. Ng, S. Jin, and B. Ai, "Improving sum-rate of cell-free massive MIMO with expanded compute-and-forward," *IEEE Trans. Signal Process.*, vol. 70, no. 12, pp. 202-215, Dec. 2021.
- [8] X. Chen *et al.*, "Energy efficiency of wireless-powered cell-free mMIMO with hardware impairments," *IEEE Trans. Commun.*, early access, Feb. 2024.
- [9] S. Chen, J. Zhang, E. Björnson, J. Zhang, and B. Ai, "Structured massive access for scalable cell-free massive MIMO systems," *IEEE J. Sel. Areas Commun.*, vol. 39, no. 4, pp. 1086-1100, Apr. 2021.
- [10] E. Björnson and L. Sanguinetti, "Making cell-free massive MIMO competitive with MMSE processing and centralized implementation," *IEEE Trans. Wireless Commun.*, vol. 19, no. 1, pp. 77-90, Jan. 2019.
- [11] Z. Wang, J. Zhang, H. Q. Ngo, B. Ai, and M. Debbah "Uplink precoding design for cell-free massive MIMO with iteratively weighted MMSE," *IEEE Trans. Commun.*, vol. 71, no. 3, pp. 1646 - 1664, Mar. 2023.
- [12] Q. Sun *et al.*, "Uplink performance of hardware-impaired cell-free massive MIMO with multi-antenna users and superimposed pilots," *IEEE Trans. Commun.*, vol. 71, no. 11, pp. 6711-6726, Nov. 2023.
- [13] J. Zhang *et al.*, "Performance analysis and optimization of NOMA-based cell-free massive MIMO for IoT," *IEEE Internet Things J.*, vol. 9, no. 12, pp. 9625-9639, Nov. 2021.
- [14] *Identification and Quantification of Key Socio-Economic Data to Support Strategic Planning for the Introduction of 5G in Europe*, Europe Union, Brussels, Belgium, 2016.
- [15] R. Long, Y.-C. Liang, H. Guo, G. Yang, and R. Zhang, "Symbiotic radio: A new communication paradigm for passive Internet of Things," *IEEE Internet Things J.*, vol. 7, no. 2, pp. 1350-1363, Feb. 2020.
- [16] J. Xu, Z. Dai, and Y. Zeng, "MIMO symbiotic radio with massive backscatter devices: Asymptotic analysis and precoding optimization," *IEEE Trans. Commun.*, vol. 71, no. 9, pp. 5487-5502, Sept. 2023.
- [17] Y.-C. Liang, Q. Zhang, E. G. Larsson, and G. Y. Li, "Symbiotic radio: Cognitive backscattering communications for future wireless networks," *IEEE Trans. Cognit. Commun. Netw.*, vol. 6, no. 4, pp. 1242-1255, Dec. 2020.
- [18] Q. Zhang, Y.-C. Liang, H. -C. Yang, and H. V. Poor, "Mutualistic mechanism in symbiotic radios: When can the primary and secondary transmissions be mutually beneficial?" *IEEE Trans. Wireless Commun.*, vol. 21, no. 10, pp. 8036-8050, Oct. 2022.
- [19] Z. Dai, R. Li, J. Xu, Y. Zeng, and S. Jin, "Rate-Region characterization and channel estimation for cell-free symbiotic radio communications," *IEEE Tran. Commun.*, vol. 71, no. 2, pp. 674-687, Feb. 2023.
- [20] M. Ataeshojai, R. C. Elliott, W. A. Krzymieñ, C. Tellambura, and I. Maljević, "Symbiotic backscatter communication underlying a cell-free massive MIMO system," *IEEE Internet Things J.*, vol. 10, no. 19, pp. 16758 - 16777, Oct. 2023.
- [21] F. Li, Q. Sun, X. Chen, and J. Zhang, "Spectral efficiency analysis of uplink cell-free massive MIMO symbiotic radio," *IEEE Internet Things J.*, vol. 11, no. 2, pp. 3614 - 3627, Jan. 2024.
- [22] T. Zhang *et al.*, "Rate-splitting with hybrid messages: DoF analysis of the two-user MIMO broadcast channel with imperfect CSIT," *IEEE Trans. Wireless Commun.*, early access, Mar. 2024.
- [23] J. Park *et al.*, "Rate-splitting multiple access for 6G networks: Ten promising scenarios and applications," *IEEE Network*, early access, Oct. 2023.
- [24] H. Joudeh and B. Clerckx, "Sum-rate maximization for linearly precoded downlink multiuser MISO systems with partial CSIT: A rate-splitting approach," *IEEE Trans. Commun.*, vol. 64, no. 11, pp. 4847-4861, Nov. 2016.
- [25] S. Park, J. Choi, J. Park, W. Shin, and B. Clerckx, "Rate-splitting multiple access for quantized multiuser MIMO communications," *IEEE Trans. Wireless Commun.*, vol. 22, no. 11, pp. 7696-7711, Nov. 2023.
- [26] S. H. Chae, H. W. Kim, H. J. Park, and S.-W. Jeon, "Rate splitting-based hybrid beamforming for multi-user downlink cellular networks," *IEEE Trans. Commun.*, early access, Feb. 2024.
- [27] B. Clerckx, H. Joudeh, C. Hao, M. Dai, and B. Rassouli, "Rate splitting for MIMO wireless networks: a promising PHY-layer strategy for LTE evolution," *IEEE Commun. Mag.*, vol. 54, no. 5, pp. 98-105, May 2016.
- [28] Y. Mao, B. Clerckx, and V. O. K. Li, "Rate-splitting multiple access for downlink communication systems: Bridging, generalizing, and outperforming SDMA and NOMA," *EURASIP J. Wireless Commun. Netw.*, vol. 2018, no. 1, p. 133, May 2018.
- [29] A. Mishra, Y. Mao, O. Dizdar, and B. Clerckx, "Rate-splitting multiple access for downlink multiuser MIMO: Precoder optimization and PHY-layer design," *IEEE Trans. Commun.*, vol. 70, no. 2, pp. 874-890, Feb. 2022.
- [30] X. Lyu, S. Aditya, J. Kim, and B. Clerckx, "Rate-splitting multiple access: The first prototype and experimental validation of its superiority over SDMA and NOMA," *IEEE Trans. Wireless Commun.*, early access, Mar. 2024.
- [31] B. Clerckx *et al.*, "A primer on rate-splitting multiple access: Tutorial, myths, and frequently asked questions," *IEEE J. Sel. Areas Commun.*, vol. 41, no. 5, pp. 1265-1308, May 2023.
- [32] H. Niu *et al.*, "Active RIS assisted rate-splitting multiple access network: Spectral and energy efficiency tradeoff," *IEEE J. Sel. Areas Commun.*, vol. 41, no. 5, pp. 1452-1467, May 2023.
- [33] O. Dizdar, Y. Mao, and B. Clerckx, "Rate-splitting multiple access to mitigate the curse of mobility in massive MIMO networks," *IEEE Trans. Commun.*, vol. 69, no. 10, pp. 6765-6780, Jul. 2021.
- [34] A. Mishra, Y. Mao, C. K. Thomas, L. Sanguinetti, and B. Clerckx, "Mitigating intra-cell pilot contamination in massive MIMO: A rate splitting approach," *IEEE Trans. Wireless Commun.*, vol. 22, no. 5, pp. 3472-3487, May 2023.
- [35] J. Zheng *et al.*, "Asynchronous cell-free massive MIMO with rate-splitting," *IEEE J. Sel. Areas Commun.*, vol. 41, no. 5, pp. 1366-1382, May 2023.
- [36] A. Mishra, Y. Mao, L. Sanguinetti, and B. Clerckx, "Rate-splitting assisted massive machine-type communications in cell-free massive MIMO," *IEEE Commun. Lett.*, vol. 26, no. 6, pp. 1358-1362, Jun. 2022.
- [37] J. Zheng *et al.*, "Rate-splitting for CF massive MIMO systems with channel aging," *IEEE Trans. Veh. Technol.*, vol. 73, no. 1, pp. 1485-1490, Jan. 2024.
- [38] A. Lin, "Binary search algorithm," *WikiJ. Sci.*, vol. 2, no. 1, pp. 1-13, Jan. 2019.
- [39] Ö. Özdogan, E. Björnson, and J. Zhang, "Cell-free massive MIMO with Rician fading and phase shifts," *IEEE Trans. Wireless Commun.*, vol. 18, no. 11, pp. 5299-5315, Nov. 2019.
- [40] Z. Wang, J. Zhang, E. Björnson, and B. Ai, "Uplink performance of cell-free massive MIMO over spatially correlated Rician fading channels," *IEEE Commun. Lett.*, vol. 25, no. 4, pp. 1348-1352, Apr. 2021.



Feiyang Li received the B.S. degree from the College of Information Science and Technology, Nantong University, Nantong, China, in 2021. He is currently pursuing the Ph.D. degree with Nantong University. His research interests include massive MIMO systems, backscatter communication, and performance analysis of wireless communication systems.



Qiang Sun (Member, IEEE) received the Ph.D. degree in communications and information systems from Southeast University, Nanjing, China, in 2014. He was a Visiting Scholar with the University of Delaware, Newark, DE, USA, in 2016. He is currently a Professor with the School of Information Science and Technology, Nantong, China. His research interests include deep learning and wireless communications. He was a member of Technical Program Committee and a reviewer for a number of IEEE conferences/journals.



Xiaomin Chen (Member, IEEE) received the B.S. and the M.S. degrees in communications engineering from Tongji University, Shanghai, China, in 2005 and 2008, respectively, and the Ph.D. degree (Hons.) in electronic engineering from Technische Universität Braunschweig, Germany, in 2014. She is currently with the School of Information Science and Technology, Nantong University, Nantong, China. Her research interests include error-control coding, wireless networks, and machine learning in communication systems.

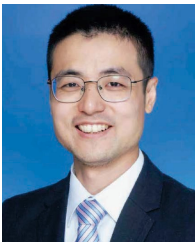


Kai-Kit Wong (Fellow, IEEE) (M'01-SM'08-F'16) received the BEng, the MPhil, and the PhD degrees, all in Electrical and Electronic Engineering, from the Hong Kong University of Science and Technology, Hong Kong, in 1996, 1998, and 2001, respectively. After graduation, he took up academic and research positions at the University of Hong Kong, Lucent Technologies, Bell-Labs, Holmdel, the Smart Antennas Research Group of Stanford University, and the University of Hull, UK. He is Chair in Wireless Communications at the Department of Electronic and Electrical Engineering, University College London, UK. His current research centers around 6G and beyond mobile communications. He is Fellow of IEEE and IET. He served as the Editor-in-Chief for IEEE Wireless Communications Letters between 2020 and 2023.



Shuping Dang (Senior Member, IEEE) received B.Eng (Hons) in Electrical and Electronic Engineering from the University of Manchester (with first class honors) and B.Eng in Electrical Engineering and Automation from Beijing Jiaotong University in 2014 via a joint '2+2' dual-degree program. He also received D.Phil in Engineering Science from University of Oxford in 2018. Dr. Dang joined in the R&D Center, Huanan Communication Co., Ltd. after graduating from University of Oxford and worked as a Postdoctoral Fellow with the Computer,

Electrical and Mathematical Science and Engineering Division, King Abdullah University of Science and Technology (KAUST). He is currently a Lecturer with School of Electrical, Electronic and Mechanical Engineering, University of Bristol. The research interests of Dr. Dang include 6G communications, wireless communications, wireless security, and machine learning for communications.



Jiayi Zhang (Senior Member, IEEE) received the B.Sc. and Ph.D. degree of Communication Engineering from Beijing Jiaotong University, China in 2007 and 2014, respectively.

Since 2016, he has been a Professor with School of Electronic and Information Engineering, Beijing Jiaotong University, China. From 2014 to 2016, he was a Postdoctoral Research Associate with the Department of Electronic Engineering, Tsinghua University, China. From 2014 to 2015, he was also a Humboldt Research Fellow in Institute for Digital

Communications, Friedrich-Alexander-University Erlangen-Nürnberg (FAU), Germany. From 2012 to 2013, he was a visiting scholar at the Wireless Group, University of Southampton, United Kingdom. His current research interests include cell-free massive MIMO, reconfigurable intelligent surface (RIS), communication theory and applied mathematics. Dr. Zhang received the Best Paper Awards at the WCSP 2017 and IEEE APCC 2017, the URSI Young Scientist Award in 2020, and the IEEE ComSoc Asia-Pacific Outstanding Young Researcher Award in 2020. He was recognized as an exemplary reviewer of the IEEE COMMUNICATIONS LETTERS in 2015-2017. He was also recognized as an exemplary reviewer of the IEEE TRANSACTIONS ON COMMUNICATIONS in 2017-2019. He was the Lead Guest Editor of the special issue on "Multiple Antenna Technologies for Beyond 5G" of the IEEE JOURNAL ON SELECTED AREAS IN COMMUNICATIONS and an Editor for IEEE COMMUNICATIONS LETTERS from 2016-2021. He currently serves as an Associate Editor for IEEE TRANSACTIONS ON COMMUNICATIONS, IEEE ACCESS and IET COMMUNICATIONS.